Hindawi
Journal of Nanomaterials
Volume 2018, Article ID 9301912, 12 pages
https://doi.org/10.1155/2018/9301912

Research Article

Assessment of Charged AuNPs: From Synthesis to Innate Immune Recognition

K. Rahme,[1] **G. Minassian**,[1] **M. Sarkis**,[1] **M. Nakhl**,[2] **R. El Hage**,[2] **E. Souaid**,[2] **J. D. Holmes**,[3] **and E. Ghanem**[1]

[1]*Department of Sciences, Faculty of Natural and Applied Sciences, Notre Dame University-Louaize, Zouk Mosbeh, Lebanon*
[2]*Faculty of Sciences, Fanar Campus, Chemistry & Physics Department, and Doctoral School, Lebanese University, Beirut, Lebanon*
[3]*Materials Chemistry and Analysis Group, School of Chemistry and the Tyndall National Institute, University College Cork, Cork, Ireland*

Correspondence should be addressed to K. Rahme; kamil.rahme@ndu.edu.lb

Received 13 April 2018; Revised 24 July 2018; Accepted 8 August 2018; Published 3 September 2018

Academic Editor: Enrico Bergamaschi

Gold nanoparticle (AuNP) physicochemical characteristics, mainly size and charge, modulate their biodistribution, cytotoxicity, and immunorecognition as reported from *in vitro* and *in vivo* studies. While data from *in vitro* studies could be biased by several factors including activation of cells upon isolation and lack of sera proteins in the microenvironment of primary generated cell lines, *in vivo* studies are costly and time-consuming and require ethics consideration. In this study, we developed a simple and novel *in vivo*-like method to test for NP immunorecognition from freshly withdrawn human blood samples. AuNPs with a size range of 30 ± 5 nm coated with cationic poly($_L$-lysine) (PLL) dendrigraft and slightly negative poly(vinyl alcohol) (PVA) were synthesized in water. PLL-capped AuNPs were further coated with poly(ethylene glycol) (PEG) to obtain nearly neutrally charged PEG-AuNPs. Physicochemical properties were determined using zeta potential measurements, UV-Vis spectroscopy, dynamic light scattering (DLS), and scanning electron microscopy (SEM). Gel electrophoretic separation, zeta potential, and DLS were also used to characterize our NPs after human blood plasma treatment. PLL-AuNPs showed similar variation in charge and binding affinity to plasma proteins in comparison with PVA-AuNPs. However, PLL-AuNPs.protein complexes revealed a drastic change in size compared to the other tested particles. Results obtained from the neutrophil function test and pyridine formazan extraction revealed the highest activation level of neutrophils (~70%) by 50 μg/mL of PLL-AuNPs compared to a null induction by PEG- and PVA-AuNPs. This observation was further verified by flow cytometry analysis of polymorphonuclear cell size variation in the presence of coated AuNPs. Overall, our *in vivo*-like method, to test for NP immunorecognition, proved to be reliable and effective. Finally, our data supports the use of PEG-AuNPs as promising vehicles for drug delivery, as they exhibit minimal protein adsorption affinity and insignificant charge and size variation once introduced in whole blood.

1. Introduction

In the dawn of a new era of biomedical advancements, nanotechnology has paved the way to manipulate and tailor matters at the nanometer scale, which permits the engineering of a wide array of nanomaterials [1, 2]. Engineered nanoparticles (NPs), particularly gold nanoparticles (AuNPs), are one of the most commonly studied substances due to their widespread use in biomedical applications, cosmetics, and cancer treatment [3–7]. AuNPs exhibit attractive physicochemical and optical properties, fast biodistribution, and dose-dependent cytotoxicity [8–11]. However, for effective clinical applications, AuNPs should evade the first line of innate immunity mediated particularly by polymorphonuclear cells (PMNs) [12, 13].

Therefore, NPs must be well designed and properly coated to cross the immune barrier and ensure optimum trafficking to a targeted site with minimal cytotoxicity [14, 15]. The immunogenic effects of nanoparticles are mainly attributed to their charge, size, and type [16–18]. In alignment with

this observation, Hwang et al. [19] mentioned that the inflammatory immune responses are largely dependent on the nature of cationic additives in nanosystems. Lockman et al. [20] demonstrated that cationic carbon NPs exert toxicity at the blood brain barrier while anionic and neutral NPs did not. Furthermore, Moyano et al. [21] showed that neutral tetraethylene glycol (TEG) AuNPs do not elucidate inflammatory responses in an *in vivo* mouse model. Bartneck et al. [22] highlighted the fact that charge rather than size affects the capacity of NPs to be trapped. For instance, positively charged CTAB-coated gold nanorods (NRs) significantly enhanced cellular uptake by neutrophils, while negatively charged PEO-NRs did not [22]. Thus, CTAB NRs might not escape the inflammatory response by phagocytes prior to their extravasation to the target site for their ligand release.

On the other hand, nanomaterials of different morphologies, such as carbon nanotubes, yet of similar composition exhibit different biological responses regarding inflammation and injury to cells, concomitant to macrophage and neutrophil accumulation [23]. It was also reported that colloidal AuNPs injected into mice enhanced the proliferation of lymphocytes [9]. Other studies revealed size-dependent uptake and cytokine release of bare AuNPs by human dendritic cells [24]. Moreover, AuNPs at sizes ranging from 15 to 50 nm might undergo phagocytosis by monocytes and trapping via neutrophil extracellular traps (NETs) [22]. In addition, even smaller sizes of AuNPs (5 to 35 nm) showed *in vitro* internalization by human leukemia macrophages [25].

As noted above, NP immunorecognition can be monitored using different methods, such as lymphocyte proliferation, neutrophil function test (NFT) [26], NET formation, cytokine release, phagocytosis/internalization activity, and sera antibody measurements [27–31]. Methods can be conducted *in vitro* or *in vivo* using animal models. *In vitro* studies mainly depend on the isolation of primary cell lines or the utilization of immortal transformed cell lines [32–35]. However, such cell lines do not mimic *in vivo* physiological conditions and might result in false-positive observations due to the activation of immune cells during isolation or the lack of sera proteins that might affect immune recognition via opsonization [36–38]. *In vivo* studies, on the other hand, are quite expensive, complex in their experimental setup, and time demanding and require a high level of ethics consideration [14, 39]. Given that slight changes to the coating and size of AuNPs might elicit different immune responses, we employed an *in vivo*-like method that is rapid, reliable, and cheap to investigate the interaction of the phagocytes, particularly neutrophils, with various charged polymer-capped AuNPs, namely, with cationic poly($_L$-lysine) (PLL) dendrigraft, slightly negative poly(vinyl alcohol) (PVA), and nearly neutral poly(ethylene glycol) (PEG) coats with the aim of strengthening our knowledge on charged AuNPs and their effect on immune cells. Finally, we speculate based on previous results and other reports that loading AuNPs with polymers such as PEG and PVA would create a stable protective hydrophilic layer that reduces their recognition and uptake by PMNs and enhances their longevity in circulation [40–44]. However, cationic PLL-AuNPs will trigger a pronounced immune response since positively charged polymers have the tendency to bind to negatively charged membranes triggering activation and endocytosis [45, 46].

In our study, the properties of PLL-, PVA-, and PEG-coated AuNPs were characterized using zeta potential measurements, UV-Vis spectroscopy, dynamic light scattering, and scanning electron microscopy. To address the immunogenicity of NPs, we investigated the activation efficiency of neutrophils by charged NPs using nitrotetrazolium blue (NBT) dye reduction and pyridine extraction of formazan granules from a freshly withdrawn human blood sample. Flow cytometry was used to confirm the morphological changes upon neutrophil activation with charged AuNPs. In contrast to what is already reported in the literature, AuNPs—if coated with PVA or PEG—can resist phagocytosis, serving as potential noncytotoxic vehicles in medical and healthcare applications.

It is worth noting that the surface charge of our tested NPs might be affected by plasma protein adsorption upon incubation with human whole blood, consequently altering the size of the polymer-AuNPs.protein complexes. This notion is addressed in our manuscript in an attempt to understand whether the surface charge has a direct or indirect effect in neutrophil NPs' recognition.

2. Materials and Methods

2.1. Chemicals. Purified H_2O (resistivity ≈ 18.2 MΩ·cm) was used as a solvent. All glassware was cleaned with aqua regia (3 parts of concentrated HCl and 1 part of concentrated HNO_3), rinsed with distilled water, ethanol, and acetone, and oven dried before use. Tetrachloroauric acid trihydrate ($HAuCl_4$, $3H_2O$), $_L$-ascorbic acid, phorbol myristate acetate (PMA), nitrotetrazolium blue (NBT), poly(vinyl alcohol) (PVA), and thiolated pyridine were purchased from Sigma-Aldrich. Thiol-terminated poly(ethylene glycol) methyl ether, $M_w = 5400$, was purchased from Polymer Source. Poly($_L$-lysine) (PLL) dendrigraft with an average molecular weight of 7 KD was synthesized and characterized by a previously reported method [47]. Red blood cell lysis buffer was purchased from Partec. All chemicals were used as received without further purification.

2.2. Synthesis of Charged Gold (Au) Nanoparticles

2.2.1. Synthesis of PLL-AuNPs. In a 50 mL round flask containing 22.07 mL of deionized water, 0.336 mL $HAuCl_4$ (18.6 mM) was added under stirring, followed by the fast addition of 2.5 mL of PLL (100 μM) as a stabilizing ligand and 0.097 mL of ascorbic acid (0.1 M) as a reducing agent. After addition of ascorbic acid, the color of the solution changed from pale yellow to red. The solution was kept under stirring for 24 hours. The obtained nanoparticles have a hydronamic diameter of about 47.5 ± 0.3 nm (size by intensity) and a zeta potential of $+33 \pm 2.5$ mV.

2.2.2. Synthesis of PVA-AuNPs. In a 50 mL round flask containing 24.07 mL of deionized water, 0.336 mL $HAuCl_4$ (18.6 mM) was added under stirring, followed by the fast addition of 0.5 mL of PVA (0.091% *w*/*v*) as a stabilizing

ligand and 0.097 mL of ascorbic acid (0.1 M) as a reducing agent. After addition of ascorbic acid, the color of the solution changed from pale yellow to deep red. The solution was kept under stirring for 24 hours. The obtained nanoparticles had a hydronamic diameter of about 59.0 ± 6.0 nm (size by intensity) and a zeta potential of -9 ± 1 mV.

2.2.3. Synthesis of PEG-AuNPs by PEGylation of PLL-AuNPs. To 5 mL of PLL-AuNP colloidal solution under stirring, 0.27 mL of SH-PEG5000 (111 μM) was added drop wise during 3 mins and the solution was kept under stirring for two hours. The successful PEGylation was confirmed by DLS where the size of the PLL-AuNPs was found to increase from 47.5 ± 0.3 nm (size by intensity) to 75.26 ± 0.76 nm while the zeta potential was found to decrease from $+33 \pm 2.5$ mV to $+12.0 \pm 3$ mV, confirming the attachment of PEG onto the PLL-AuNP surface.

2.3. Avoiding Endotoxin Contamination. Due to the ubiquitous presence of endotoxin in all chemicals and glassware used in laboratories [48] and its interference in immunosafety results [49], appropriately adopted practices were taken into consideration for avoiding/restricting endotoxin contamination [50]. Effective methods included working under laminar flow hood with gloves and autoclaved glasses after cleaning with aqua regia and ethanol; moreover, deionized water was double autoclaved and nonpyrogenic plastics were used similarly for all sample preparation. We believe that such practices are safer than dry heating our NPs at high temperatures as the latter might affect the AuNP physicochemical characteristics [51].

2.4. Scanning Electron Microscopy (SEM). Gold nanoparticles were deposited from solution on a silicon wafer and dried in air prior to inspection by scanning electron microscopy (SEM). The samples were inspected using a Hitachi S-4300 environmental scanning electron microscope (ESEM) operating at 10 kV. Samples were metalized with carbon to avoid charging during observation.

2.5. Dynamic Light Scattering and Zeta Potential Measurements. The size distribution and surface charge (zeta potential) of the AuNP colloidal solutions were determined by dynamic light scattering (DLS) with the Malvern Zetasizer Nano ZSP using the default NIBS 173° backscattering technique. The model used in the fitting procedure was based on Mark–Houwink parameters; all the data was fitted using the cumulative fit given by the suppliers. Measurements were performed on the pristine solutions of AuNPs (50 μg/mL) using disposable folded capillary cuvettes at 25°C. Triplicates of each sample have been made for result comparison efficiency.

2.6. Incubation of AuNPs with Human Blood Plasma. Human blood was collected intravenously from three different individuals ($n = 3$) and collected in either EDTA or lithium heparin tubes to prevent coagulation. Blood samples were centrifuged at 1000 g for 5 mins to allow the serum to separate. After centrifugation, human serum was incubated with 3 differently charged AuNPs (50 μg/mL) (PLL, PVA, and PEG) at a 1 : 1 ratio at 37°C for 15 mins. The samples were then centrifuged at 8000 rpm for 10 mins to pellet down the AuNPs.protein complexes. The excess serum was removed, and the pellet was washed 3 times then resuspended in deionized water.

2.7. DLS and Zeta Measurements of AuNPs.protein Complexes. 500 μL of each AuNPs.protein complex was withdrawn for DLS and zeta measurements. The readings were done in triplicate for statistical significance and were compared with the previous readings of AuNPs prior to plasma incubation.

2.8. 1-D Gel Electrophoresis. A 12% SDS-polyacrylamide gel was prepared. The samples were pelleted down after washing and were resuspended with an SDS buffer at a concentration of 50 μg/mL containing 2% SDS, 5% β-mercaptoethanol, 10% glycerol, and 62.5 mM Tris-HCl. After heating at 95°C for 5 mins, 20 μL of each sample was transferred to each well of the previously prepared gel, with human serum (1 : 1000) being a control. Gels were run at a constant voltage of 200 V for 45 mins and stained using a solution of Coomassie Blue protein stain. Gels were imaged with ChemiDoc-It Imaging System using VisionWorks LS analysis software.

2.9. Neutrophil Function Test and Microscopic Examination. 1 mL of whole human blood was withdrawn via intravenous injection and stored in EDTA tubes. 100 μL of blood was transferred to an eppendorf tube containing 50 μL of 1 mg/mL NBT (nitrotetrazolium blue) and 50 μL of differently charged AuNPs (50 μg/mL) or with PMA as a positive control. The mixture was then incubated at 37°C for 15 mins. Smears where then fixed using 1 mL ice-cold methanol and left to dry at room temperature. Finally, smears were stained using the Wright's stain technique (eosin-methylene blue) and observed under a light microscope at 40x and 100x.

2.10. Preparing Cells for Flow Cytometry Analysis. 100 μL of EDTA whole blood was transferred to a FACS cuvette containing 50 μL of 1 mg/mL NBT dye and 50 μL of one of the charged AuNPs (50 μg/mL). PBS and PMA served as a negative control and positive control, respectively. Samples were then incubated at 37°C for 15 mins. In addition, 100 μL of 4% PFA was added to all samples which have been left to incubate in the dark for another 10 mins. Finally, the volume of the samples was brought up to 1 mL using 1x PBS (700 mL). Samples were read using a Partec Cube 8 flow cytometer with gates set at 2×10^5 particles, and data was analyzed using FlowJo.

2.11. Pyridine Extraction and Spectrophotometry. Pyridine extraction was done using the same protocol adopted for FACS analysis. 100 μL of blood was used for each sample mixed with 50 μL of one type of the charged AuNPs (50 μg/mL) PLL, PVA, and PEG and 50 μL of 1 mg/mL NBT. Samples were then incubated at 37°C for 15 mins, fixed with 4% PFA, and incubated with RBC lysis buffer for 20 mins. Afterwards, samples were centrifuged at 400 g for 10 mins, the supernatant was discarded, and the pellet was resuspended with 0.5 mL of 99% pyridine and 0.5 mL $1 \times$ PBS to extract formazan deposits. Formazan absorbance

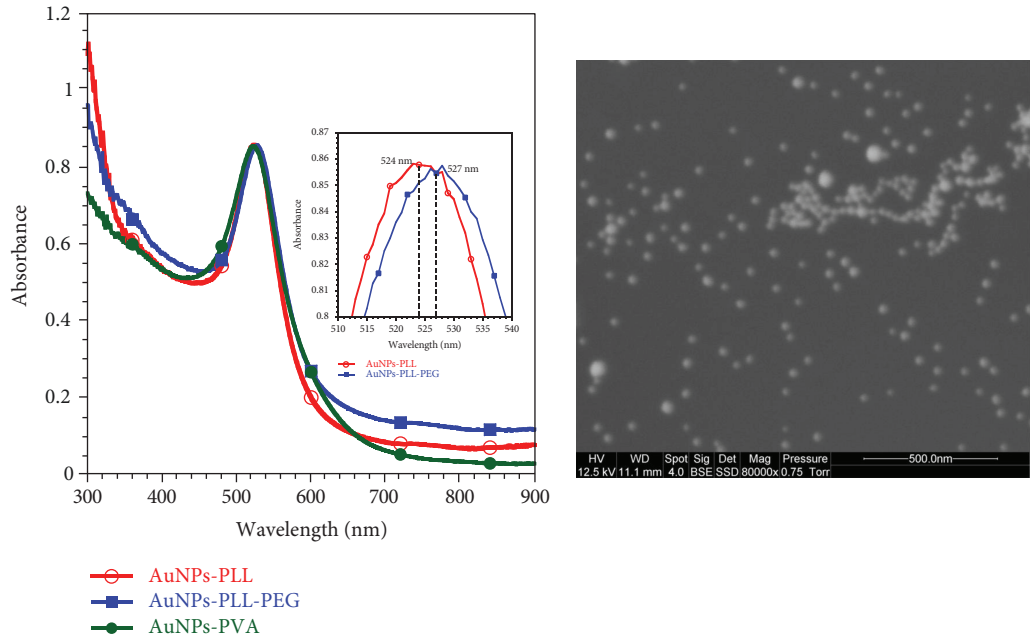

(a) (b)

Figure 1: (a) UV-visible spectra of different AuNPs synthesized in this study (absorbance adjusted to the same value); the inset shows the clear red shift of about 3 nm before and after PEGylation of PLL-AuNPs. (b) SEM image of PLL-AuNPs with a diameter of about 30 nm (scale bar 500 nm).

was measured at 515 nm using a SPECORD 250 PLUS spectrophotometer. Finally, data measurements were normalized using a basic statistical formula where the normalized value $z = (xi - \min(x))/(\max(x) - \min(x))$, where $\min(x)$ corresponds to lowest value of the PBS data set and $\max(x)$ corresponds to the highest value of the PMA data set and (xi) stands for the value to be normalized. The results were plotted using EXCEL [52].

2.12. Statistical Analysis. The data are reported as means ± SEM and were analyzed by one-way ANOVA, and differences between tested groups and control were assessed by post hoc and Tukey's test. Statistical significance was established at $p < 0.05$, and each experiment was performed and validated at least three times. Significance was reported on each graph with $*$ representing a p value < 0.05, $**$ representing a p value less than 0.01, and $***$ representing a p value less than 0.001. *NS* corresponds to nonsignificant difference.

2.13. Ethics Statement. This study is in compliance with the recognized international standards and principles of the Declaration of Helsinki and has received ethical approval from the institutional review board (IRB) at Notre Dame University with the following reference number: IRBSU17_1_FNAS.

3. Results and Discussion

3.1. Synthesis and Characterization of Charged AuNPs. Gold nanoparticles were synthesized in water at room temperature through the chemical reduction of gold precursor ($HAuCl_4.3H_2O$) with a mid-reducing $_L$-ascorbic acid. In order to avoid uncontrolled increase in the size and to achieve a high stability of the resulting nanoparticles, PLL and PVA were added during the synthesis. The added polymers adsorb onto the growing AuNPs' surfaces and therefore allow their final size stabilization and surface charge modification. The obtained AuNPs prepared in this study were characterized by UV-visible absorption spectroscopy (Figure 1(a)) and SEM (Figure 1(b)). The UV-visible spectra clearly show a single plasmon absorbance band characteristic of highly stable spherical AuNPs; the wavelengths of maximum absorbance (λ_{max}) were found to be at 522 nm for PVA-AuNPs and 524 nm for PLL-AuNPs, indicating that their AuNP core sizes are very close to 30 ± 5 nm as determined by ImageJ analysis of the SEM image of PLL-AuNPs represented in Figure 1(b). Furthermore, thiolated polyethylene glycol (SH-PEG) is well known to further improve the biocompatibility of the nanoparticles; the SH-PEG (M_w 5400 g/mol) polymer was grafted onto Au nanoparticles through Au-SH chemical bonding. PEG attachment to the nanoparticles via ligand exchange causes a very slight red shift of about 3 nm in the plasmon absorption band as shown in the inset of Figure 1(a), and this shift is mostly due to a change of the dielectric constant at the nanoparticle surface [53].

The successful PEGylation of PLL-AuNPs was further proven by dynamic light scattering analysis and zeta potential measurements. The physicochemical properties, namely, the size by intensity, number, volume, and Z average of the colloidal AuNPs, were determined using DLS. The polydispersity

Table 1: DLS and zeta potential characterization results of PLL-, PEG-, and PVA-AuNPs.

Type of NP	Z average (d.nm)	Size by intensity (d.nm)	Size by number (d.nm)	Size by volume (d.nm)	PDI	Zeta potential (mV)
PLL-AuNP	42.5 ± 0.3	47.5 ± 0.3	31.0 ± 0.7	36.5 ± 0.50	0.115 ± 0.003	+33.8 ± 2.5
PEG-AuNP	64.3 ± 1.2	75.3 ± 0.76	38.96 ± 0.9	49.5 ± 0.98	0.175 ± 0.021	+12.0 ± 3
PVA-AuNP	54.1 ± 2.6	59.0 ± 6.0	35.85 ± 1.8	42.51 ± 5.1	0.288 ± 0.011	−9.0 ± 1.0

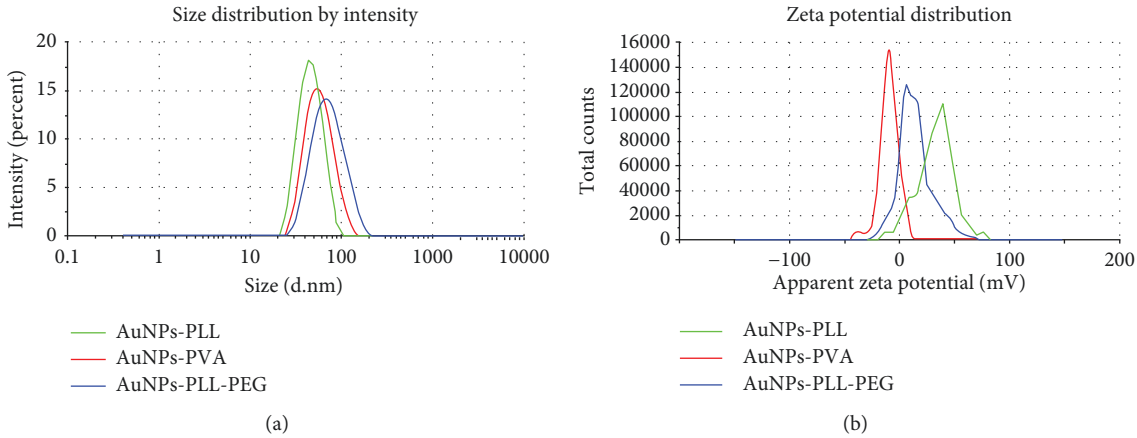

Figure 2: (a) Size distribution by intensity of PVA-AuNPs, PLL-AuNPs, and PLL-PEG-AuNPs from DLS measurements. The size of PLL-AuNPs increases from 47 nm to 75 nm after PEGylation. (b) Zeta potential for the corresponding AuNP polymers. As shown, PVA-AuNPs were slightly negative (−10 mV), while PEGylation decreased the zeta potential of the positively charged PLL-AuNPs from +34 mV to +12 mV.

index (PDI) and the resulting zeta potential from measurements were also noted as shown in Table 1. Figure 2 shows the size distribution by intensity (Figure 2(a)) and the zeta potential measurements of the corresponding colloidal solutions (Figure 2(b)). In brief, DLS measurements have shown that the synthesized AuNPs were nearly monodisperse with a single size distribution as shown in Figure 2(a). Furthermore, PLL-AuNPs showed a positive zeta potential of +33.8 ± 2.5 mV, indicating that they were successfully coated with PLL. The PDI of the PLL-AuNPs was found to be 0.115 ± 0.003, and the Z average was 42.5 ± 0.3 nm. The size from DLS was shown to be larger than the one from SEM; this is due to the fact that the total hydrodynamic diameter of PLL-AuNPs is measured by DLS, while in SEM, the AuNPs' core is only measured. Similarly, PVA-coated nanoparticles had a Z average diameter of 54.08 ± 2.58 nm and a polydispersity index (PDI) of 0.288 ± 0.011, slightly larger than PLL-AuNPs; indeed, their core sizes were not different. This is not surprising as the PVA molecular weight used in this study was larger and more polydispersed (13 to 30 KD) while that of PLL is smaller (7 KD); PVA-AuNPs show a zeta potential of −9.72 ± 1.33 mV. We should note that the size distribution by number was the closest to the size of the nanoparticles by SEM. PEGylation of the PLL-AuNPs was shown to increase the Z average of the PLL-AuNPs by about 22 nm (64.32 ± 1.22 nm), indicating that SH-PEG was successfully grafted onto the AuNP surface. Moreover, a decrease of the zeta potential by about 21 mV (+12 ± 3 mV) was also observed, further proving the successful attachment of PEG onto the PLL-AuNP surface.

3.2. Incubation of Polymer-Coated AuNPs with Plasma. In order to assess the plasma protein adsorption onto the different charge polymer-coated gold nanoparticles, 50 μg/mL of AuNP polymer solutions was incubated with human serum (HS) at a ratio of 1 : 1 for 15 mins at 37°C. Afterwards, the size distribution and the zeta potential were recorded. The size distribution by intensity for the different AuNP polymer solutions was obtained from DLS measurements as shown in Figure 3(a). There is a clear evidence that the non-PEGylated positively charged PLL-AuNPs increased enormously from 47.5 ± 0.3 nm to >200 nm, indicating therefore a strong interaction with plasma proteins. In contrast, nearly neutral PEGylated PLL-AuNPs increased only slightly (about 13 nm), indicating that the poly(ethylene glycol) layer plays a role in reducing or inhibiting the plasma protein adsorption onto PLL-AuNPs. The slightly negatively charged PVA-AuNPs were also shown to increase by about 80 nm after serum incubation. The zeta potential analysis after incubation shown in Figure 3(b) also demonstrated that PLL-PEG-AuNPs and PVA-AuNPs expressed a very slight change (~6 mV) in comparison to non-PEGylated positively charged PLL-AuNPs that was found to decrease from +33.8 ± 2.5 to +3 ± 0.2 mV. Next, we ran a 1-D gel electrophoresis to identify whether the physicochemical changes are mediated via protein adsorption on the surface of the NPs. Electrophoretic separation of plasma proteins from our

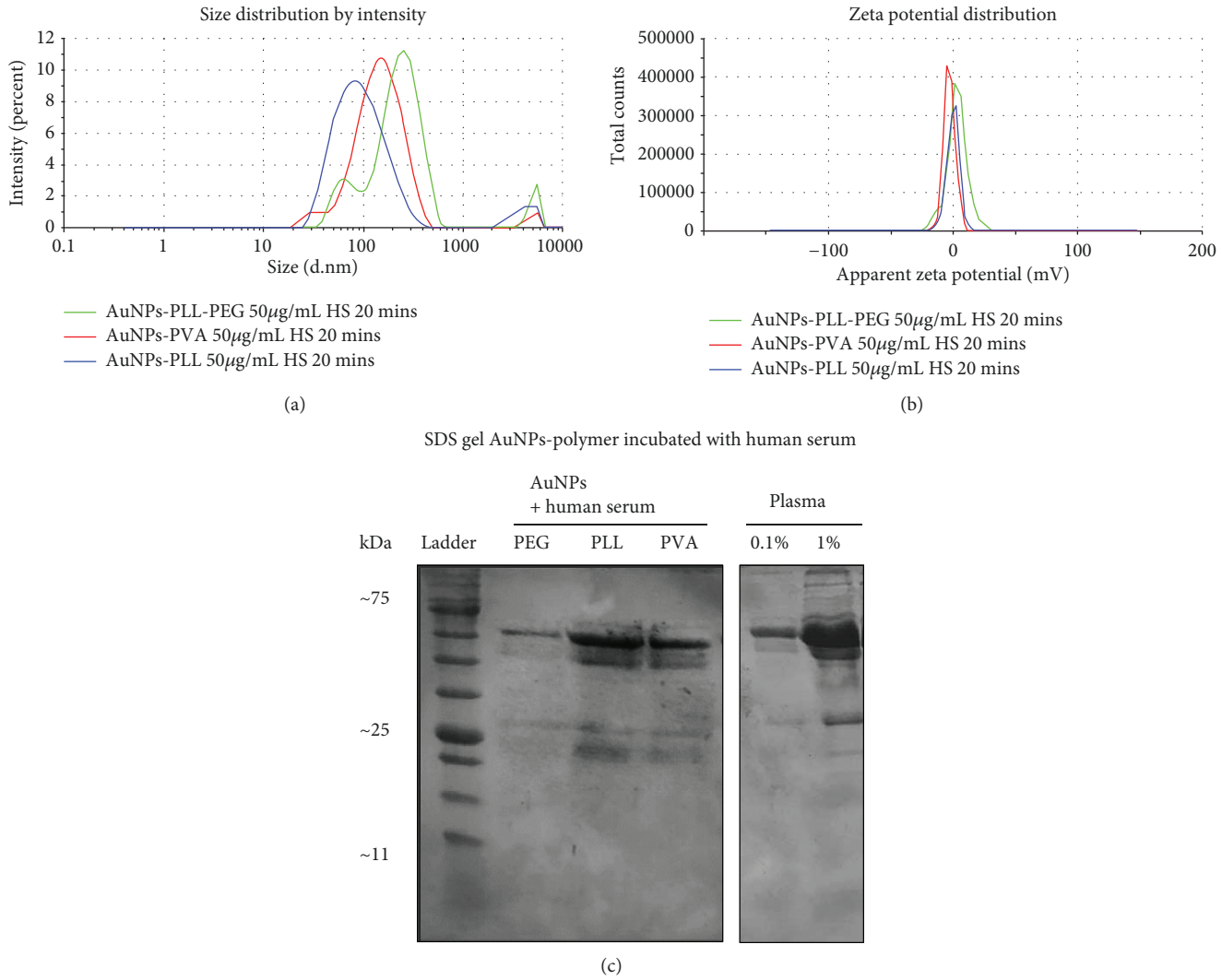

Figure 3: (a) Size distribution by intensity of AuNP polymer (50 μg/mL) from DLS measurements after incubation in human serum (HS) at a ratio of 1 : 1 for 15 mins at 37°C; the results demonstrate that the PEGylated PLL-AuNP size was the least affected by serum protein adsorption (13 nm increase only), while the non-PEGylated PLL-AuNPs increased enormously (more than 150 nm), indicating a strong interaction with plasma protein; PVA-AuNPs were also shown to increase by about 80 nm. (b) Zeta potential measurements on the corresponding AuNP polymers show that the charge of PVA-AuNPs and PLL-PEG-AuNPs witnessed a very slight change in comparison to non-PEGylated PLL-AuNPs that was found to decrease from $+33.8 \pm 2.5$ to $+3 \pm 0.2$ mV. (c) 1-D gel electrophoresis of differently charged AuNPs after incubation with human serum. A 12% SDS gel was used to visualize the difference in serum protein adsorption on charged nanoparticles. Plasma proteins at 0.1% and 1% were used for comparison. Given that human serum was undiluted during incubation, the amount of plasma serum proteins adhered to the polymer-coated nanoparticles is relatively low compared to 0.1% plasma proteins alone.

polymer-coated NPs showed comparable adsorption of proteins on PVA and PLL nanoparticles (Figure 3(c)); however, minimal binding of plasma proteins was detected on PEG particles.

We can conclude that PEGylation of positively charged PLL-AuNPs did not only decrease their zeta potential but also pulled off plasma protein adsorption resulting in very low neutrophil activation as demonstrated in Figure 4, making them suitable for *in vivo* application.

3.3. Neutrophil Function Test (NFT) and Microscopic Examination. To determine the behavior of our synthesized AuNPs under physiological conditions, we ought at testing their effect on freshly withdrawn whole blood sample. We assumed that such an environment mimics *in vivo* physiological conditions, rather than working with isolated neutrophils. The activation of PMNs, particularly neutrophils, was visualized under the microscope by monitoring the reduction of the NBT dye as depicted in Figure 4. NBT is a colorless/slightly yellow dye that is often used in standard neutrophil activation tests. It is used to quickly and easily calculate the percentage of activated neutrophils in peripheral blood [54]. Upon incubation with the presence of a neutrophil-activating substance, such as phorbol myristate acetate (PMA), NBT is reduced by the NADPH oxidase pathway in neutrophils becoming dark blue-grey in color. This change in color is due to the reduction of NBT to formazan deposits [55, 56]. In the present paper, basic light microscopy was used

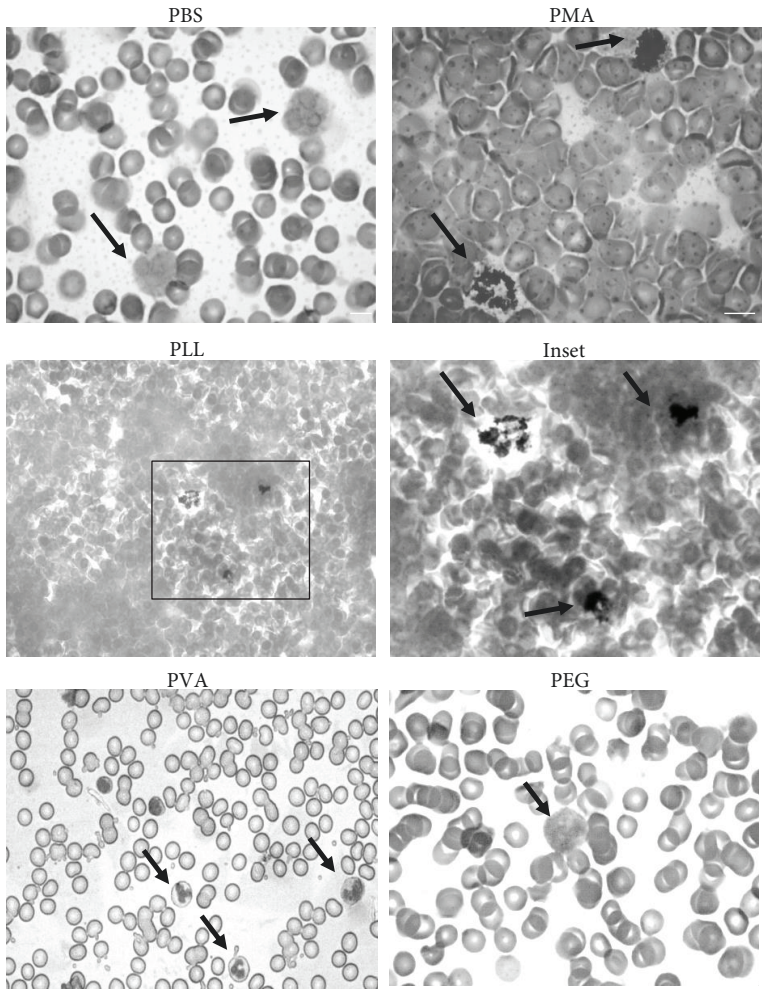

Figure 4: Microscopic observation of AuNP interaction with human neutrophils. Whole blood was withdrawn intravenously from a 22-year-old adult in a healthy condition. Blood was mixed with EDTA (1 : 1 ratio) prior to its incubation with different charged NPs for 15 mins at 37°C in the presence of nitro blue tetrazolium (NBT) dye. Cells were then smeared and stained with eosin and methylene blue and observed under light microscopy. The cell density of polymorphonuclear (PMN) cells was relatively similar in both thick and thin smears, regardless of erythrocytes' concentration. Black arrows point to PMNs. PBS: negative control; PMA positive control; poly($_L$-lysine) (PLL): positively charged NPs; poly(vinyl alcohol) (PVA): negatively charged NPs; poly(ethylene glycol) (PEG): neutral NPs. Activated neutrophils exhibited formazan granules in the presence of PMA and PLL as further depicted in the enlarged inset. Scale bar: 10 μm ($n = 6$).

to identify the amount of formazan deposits in the cytoplasm of neutrophils, hence deducing their percent activation.

To quantify the percent of activation, formazan deposits were observed from three different experiments. In Figure 5, NFT results revealed that almost 70% of neutrophils were activated in the presence of PLL compared to 75% as activated by PMA. Activated neutrophils are clearly observed by the dark blue staining of the formazan granules deposited inside the cells and those that have been scattered and released extracellularly, while the percent of activation drastically dropped to almost 3 to 5% in the presence of negatively or neutrally charged linkers, such as PVA and PEG (Figure 5).

3.4. Flow Cytometry Analysis of Cellular Activation by AuNPs. To validate the subjective NFT results, flow cytometry analysis was selected to monitor the size increase in activated PMNs upon NP treatment. To avoid reading aggregated cells,

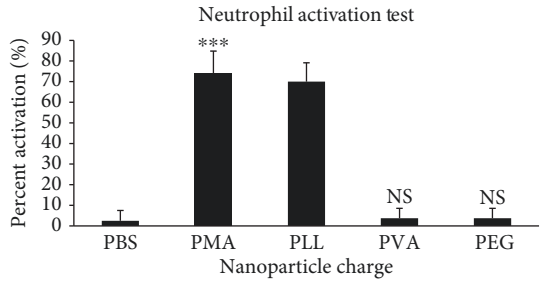

Figure 5: Neutrophil activation by various NPs. Positively charged PLL-AuNPs showed similar activation efficacy of neutrophils as compared to the control stimulant, PMA, with ~70% of activated neutrophils forming formazan deposits. PVA- and PEG-coated NPs only exhibited a 10% activation level with nonsignificant (NS) p values compared to PBS. $^{***}p$ value < 0.001 ($n = 4$).

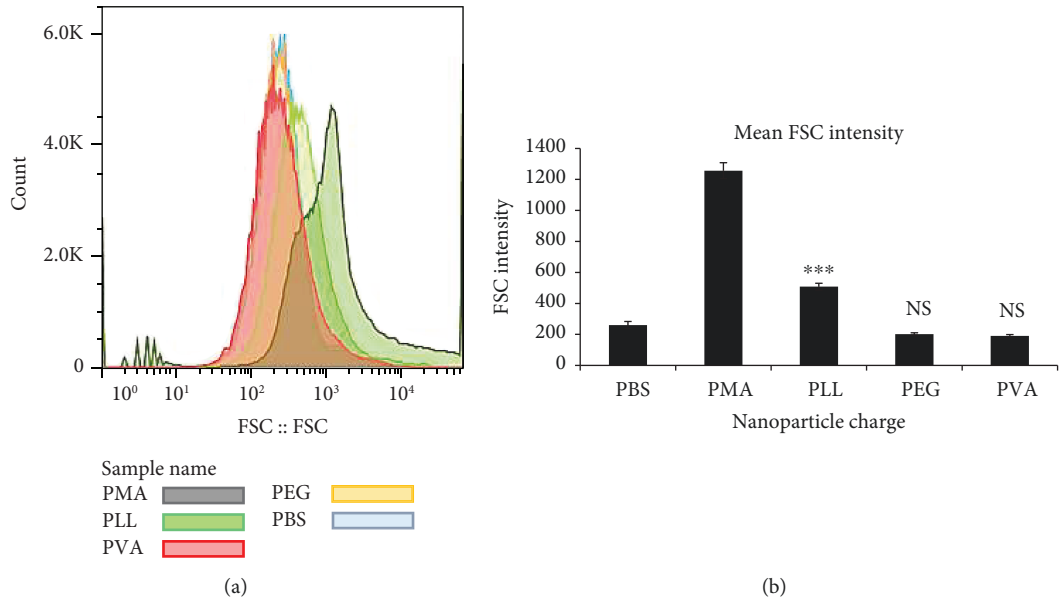

Figure 6: FACS analysis of whole blood samples in the presence of charged AuNPs. Whole blood was intravenously extracted and incubated with PBS, PMA, or various AuNPs (PLL, PVA, and PEG) at 37°C for 15 mins. Samples were then analyzed using flow cytometry. (a) Forward scatter (FSC) distribution of gated PMNs plotted using a logarithmic scale. A representative histogram with an increased FSC signal for PMA and PLL. This increase in cellular size most likely indicates the activation of polymorphonuclear cells, including neutrophils. Plots were gated at 200,000 cells per sample and extracted using FlowJo. (b) Bar chart of three replicas depicting nonsignificant (NS) p values for PEG and PVA compared to PBS. $***$ depicts a significant activation by PLL compared to PBS with a p value < 0.001.

PMNs were electronically gated based on large FSC and SSC signals and the cell density was set to 2×10^5 cells/mL. Such a cell density minimizes cell-cell adhesion that could not be analyzed through flow cytometry [12]. Histograms revealed remarkable increase in the cell volume as marked by an increase in the forward scatter of the PMA-stimulated cells. Similarly, cells treated with PLL-AuNPs showed significant increase in cell size as compared with unstimulated cells, while FSC intensity remained insignificant for cells treated with PEG and PVA-NPs (Figure 6(a)). For better quantification, mean FSC ± SEM derived from three different experiments was plotted in a bar chart (Figure 6(b)).

3.5. Formazan Granule Extraction by Pyridine. In an attempt to better analyze our results, our data set was normalized using the formula described in Materials and Methods and the percent absorbance was calculated for all samples. The experiment was repeated three times, and a blank containing a 1 : 1 ratio of deionized water (DIW) and 99% pyridine was used as a reference. As shown in Figure 7, samples incubated with PMA showed the highest percent absorbance of about 74%, followed by PLL-AuNPs with 45%. On the other hand, samples incubated with PVA-AuNPs and PEG-AuNPs displayed a percent absorbance of 12% and 14%, respectively. These values are slightly higher despite being insignificantly different to the 5% activation level pertained to the control PBS sample.

Upon exploring the interaction of NPs with the immune system's constituents, one should bear in mind many parameters such as the model organism being studied, the route of NP trafficking delivery, dose of NPs administered, and time of exposure. It is highly advisable to avoid long-term

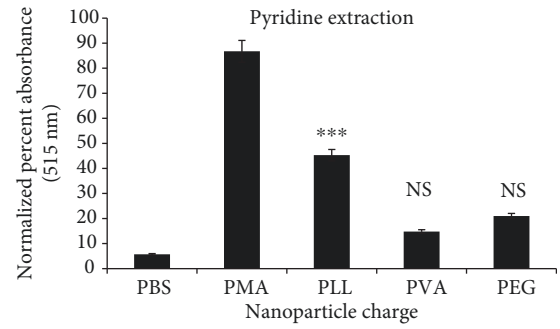

Figure 7: Determination of formazan formation after treatment of whole blood with various AuNPs. As part of neutrophil activation, formazan formation was extracted using 99% pyridine and quantified using UV-Vis spectrophotometry. The bar chart depicts highest formazan absorbance with PMA followed by PLL and insignificant absorbance with PVA and PEG ($n = 3$). $***$ depicts a significant activation by PLL compared to PBS with a p value < 0.001.

exposure and high concentrations as they can prove to be cytotoxic and induce apoptosis [57]. In order to avoid such limitations, we applied an *in vivo*-like simple and novel method that mimics physiological conditions. We believe that our method of incubating AuNPs, or any type of NP, with whole blood and observing nanoimmunogenicity either through formazan formation by neutrophils or through PMNs activation is a straightforward technique that scientists should opt for prior to actual *in vivo* studies.

Immune cells or leukocytes are mostly composed of neutrophils, as first responders to infections. They are also known to be powerful and efficient phagocytes [58]. The

neutrophil's lipid bilayer is flexible enough to undergo certain complex processes mediated by many intricate mechanisms such as "intracellular signaling cascades and many cytoskeletal rearrangements," engulfing any non-self-particle or microbe. This occurs upon ligation of neutrophil's opsonic receptors, initiating phagocytosis and ROS generation [59]. Another process exhibited by neutrophils is called "NETosis," during which the latter expels extracellular DNA traps consisting of histones, granule proteins, and free chromatin [60]. Thus, monitoring neutrophil activity in the presence of NPs reflects the tolerance of the immune system to foreign particles prior to their delivery to targeted sites.

In our study, positively charged AuNPs showed the highest activation level of neutrophils as observed by NBT reduction to dark blue formazan deposits. This correlates with a study conducted by Durocher et al. [61], demonstrating that positively charged gold nanoparticles proved to be more proinflammatory than negatively charged AuNPs.

The most common technique to assess NBT reduction is through normal light microscopy observation. However, such a technique is usually subjective as it relies on the operator's perspective and on a nonautomated mode of counting. Alternatively, we used the pyridine method to extract formazan deposits and quantify by spectrophotometry their absorbance at 515 nm [62]. In fact, it is believed that formazan deposits absorb and scatter light upon excitation [63]. Our results prior to normalization were limited by the ability of detecting the absorbance of the free roaming/nonphagocytosed gold NPs that are known to absorb light between 500 and 560 nm [64]. Another limitation was related to the optical absorbance of hemoglobin or oxyhemoglobin between 500 and 600 nm as a result of some leftover lysed RBCs in the sample preparation [65]. Both factors might interfere with spectrophotometer detection and result in false-positive values.

To confirm our results, the activation of PMNs was analyzed via the forward scatter (FSC) intensity, which indicates an increase in cell volume upon activation. Again, positively charged PLL-coated nanoparticles resulted in an increase in the PMN volume most likely due to a phagocytic response [63]. Our results align with a study conducted by Fattorossi et al. [63], demonstrating an increase in neutrophil cell size by FACS upon PMA treatment. On the other hand, the neutral and negatively charged particles PEG and PVA, respectively, did not lead to an increase in FSC; hence, no internalization occurred. If we compare the percentage of PMA-stimulated WBCs with that of the PLL treated, we will notice that both gave similar effect in the NFT results but differed in the flow cytometry analysis. This could be attributed to several factors, including (a) NFT screened only for neutrophils while flow cytometry histograms plotted all PMNs, (b) neutrophils with formazan deposits on the cell surface might score on an NFT but result in smaller size in flow cytometry due to its bursting status, and (c) PMA might be less cytotoxic than PLL to cells.

Interestingly, the difference in Z-potential of AuNPs prior to plasma incubation was no longer present in the AuNPs.protein complexes (Figure 3(b)). PLL-coated NPs lost their positivity and became nearly neutral. This inspired us to run 1-D gel electrophoresis and DLS to identify whether protein adsorption is the major contributor in neutralizing the PLL charges. Electrophoretic separation of plasma proteins from our polymer-coated NPs showed comparable adsorption of proteins on PVA and PLL nanoparticles (Figure 3(c)); however, minimal binding of plasma proteins was detected on PEGylated PLL-AuNP particles. This result is in line with a previous study showing that positively and negatively charged AuNPs incubated with human plasma resulted in a wide range of protein binding unlike the nearly neutral charged particles [66]. Our results support as well another study by Hühn et al. [67] reporting a comparable amount of bound plasma proteins on positively and negatively charged particles. The same group also tested cellular uptake of polymer-coated AuNPs and demonstrated that despite similar binding adsorption on both polymer-coated AuNPs, positively charged AuNPs are taken up faster by cells, thus pointing to the sign of charge as a major indicator in mediating internalization. It is worth noting that in our study, we used different compositions of polymers to coat our NPs, without any addition of conjugated fluorophores. We also used whole blood instead of cultured fibroblast cell lines, and yet we confirm the microscopic observation by Hühn et al. of higher rate of cellular uptake for positively charged NPs. Overall, the sign of NPs is prone to Z-potential shifts once in the blood circulation due to protein corona formation. In our case, a shift of ~+6 mV, ~−12 mV, and ~−30 mV was detected for PVA-, PEG-, and PLL-AuNPs, respectively. Interestingly, nearly neutralized PLL-AuNPs.protein complexes favored a faster activation of neutrophils compared to the negative and PEGylated NPs. This is most likely due to the change in the NPs' sizes as observed by our DLS measurements (Figure 3(a)). The highest increase of more than 200 nm was detected for positively charged PLL-AuNPs while the PEGylated PLL-AuNPs increased only by about 13 nm. Thus, aside from NPs' charge and affinity to protein adsorption, what mainly makes the difference in neutrophil activation is the NPs' size.

Therefore, our data supports the surface charge as the major determinant in attracting plasma proteins to the surface coat of the nanoparticles and consequently changing their size. The size and shape in turn are known to affect the rate of cellular uptake [68, 69]. Nearly neutral PEGylated NPs exhibit lower affinity to plasma proteins, thus reducing their size and consequently their cellular uptake, not to forget that neutrally charged NPs have less electrostatic interactions to the net negatively charged plasma membrane than do positive NPs, thereby reducing their uptake [70]. This supports other findings in the literature pointing to the use of neutral NPs (specifically PEGylated NPs) as promising agents in drug delivery [71] due to their prolonged lifetime in the blood [72, 73].

However, the inability of PEG- and PVA-coated NPs to elicit a significant immune response does not mean that AuNPs are fully inert from the immunological point of view. Such linkers might hydrolyze and degrade after an extended applied period forming metabolites or tissue lesions. This in turn might alert the immune system and trigger inflammation.

Finally, our simple method to identify the behavior of NPs in blood aliquots is quick and effective and could facilitate the immunological screening of various NPs prior to clinical applications. Next, we hope to examine the *in vivo* biodistribution of our synthesized neutral PEGylated AuNPs and their ability to be cleared in the urine or other excretory pathways [74].

4. Conclusions

It is undeniable that the future holds promising advances concerning the safe biodistribution and immune evasion of engineered nanoparticles. For the first time, this paper shows compelling evidence that reveals the immunogenic nature of charged AuNPs through the use of a novel yet simple method. Our results support the absence of a significant inflammatory activity associated with our designed gold nanoparticles, particularly PLL-AuNPs and PEG-AuNPs. Thus, such NPs serve as promising vehicles to be used for ligand or drug delivery in chronic infections, cancer treatment, and immunotherapeutic approaches.

Data Availability

The data used to support the findings of this study are available from the corresponding author upon request.

Conflicts of Interest

No potential conflict of interest was reported by the authors.

Acknowledgments

This work was supported by the National Council for Scientific Research, Lebanon, under Grant number CNRS-L-GRP2015.

References

[1] C. Blanco-Andujar, L. D. Tung, and N. T. K. Thanh, "Synthesis of nanoparticles for biomedical applications," *Annual Reports Section "A" (Inorganic Chemistry)*, vol. 106, p. 553, 2010.

[2] J. E. Gagner, S. Shrivastava, X. Qian, J. S. Dordick, and R. W. Siegel, "Engineering nanomaterials for biomedical applications requires understanding the nano-bio interface: a perspective," *Journal of Physical Chemistry Letters*, vol. 3, no. 21, pp. 3149–3158, 2012.

[3] D. P. Bai, X. F. Zhang, G. L. Zhang, Y. F. Huang, and S. Gurunathan, "Zinc oxide nanoparticles induce apoptosis and autophagy in human ovarian cancer cells," *International Journal of Nanomedicine*, vol. 12, pp. 6521–6535, 2017.

[4] M. P. Cabrera, P. E. C. Filho, C. M. C. M. Silva et al., "Highly fluorescent and superparamagnetic nanosystem for biomedical applications," *Nanotechnology*, vol. 28, no. 28, p. 285704, 2017.

[5] M. Condello, B. de Berardis, M. G. Ammendolia et al., "ZnO nanoparticle tracking from uptake to genotoxic damage in human colon carcinoma cells," *Toxicology In Vitro*, vol. 35, pp. 169–179, 2016.

[6] K. Pathakoti, M. Manubolu, and H. M. Hwang, "Nanostructures: current uses and future applications in food science," *Journal of Food and Drug Analysis*, vol. 25, no. 2, pp. 245–253, 2017.

[7] T. Dorai, Y. C. Cao, B. Dorai, R. Buttyan, and A. E. Katz, "Therapeutic potential of curcumin in human prostate cancer. III. Curcumin inhibits proliferation, induces apoptosis, and inhibits angiogenesis of LNCaP prostate cancer cells in vivo," *The Prostate*, vol. 47, no. 4, pp. 293–303, 2001.

[8] M. J. Linja, K. J. Savinainen, O. R. Saramäki, T. L. Tammela, R. L. Vessella, and T. Visakorpi, "Amplification and overexpression of androgen receptor gene in hormone-refractory prostate cancer," *Cancer Research*, vol. 61, no. 9, pp. 3550–3555, 2001.

[9] L. A. Dykman and N. G. Khlebtsov, "Immunological properties of gold nanoparticles," *Chemical Science*, vol. 8, no. 3, pp. 1719–1735, 2017.

[10] S. Jain, D. G. Hirst, and J. M. O'Sullivan, "Gold nanoparticles as novel agents for cancer therapy," *The British Journal of Radiology*, vol. 85, no. 1010, pp. 101–113, 2012.

[11] A. R. Pedrosa, J. L. Graça, S. Carvalho, M. C. Peleteiro, A. Duarte, and A. Trindade, "Notch signaling dynamics in the adult healthy prostate and in prostatic tumor development," *Prostate*, vol. 76, no. 1, pp. 80–96, 2016.

[12] S. F. van Eeden, M. E. Klut, B. A. M. Walker, and J. C. Hogg, "The use of flow cytometry to measure neutrophil function," *Journal of Immunological Methods*, vol. 232, no. 1-2, pp. 23–43, 1999.

[13] C. A. Fromen, W. J. Kelley, M. B. Fish et al., "Neutrophil–particle interactions in blood circulation drive particle clearance and alter neutrophil responses in acute inflammation," *ACS Nano*, vol. 11, no. 11, pp. 10797–10807, 2017.

[14] S. Vijayakumar and S. Ganesan, "*In vitro* cytotoxicity assay on gold nanoparticles with different stabilizing agents," *Journal of Nanomaterials*, vol. 2012, Article ID 734398, 9 pages, 2012.

[15] L. A. Dykman and N. G. Khlebtsov, "Gold nanoparticles in biology and medicine: recent advances and prospects," *Acta Naturae*, vol. 3, no. 2, pp. 34–55, 2011.

[16] T. Xia, M. Kovochich, J. Brant et al., "Comparison of the abilities of ambient and manufactured nanoparticles to induce cellular toxicity according to an oxidative stress paradigm," *Nano Letters*, vol. 6, no. 8, pp. 1794–1807, 2006.

[17] D. S. Anderson, R. M. Silva, D. Lee et al., "Persistence of silver nanoparticles in the rat lung: influence of dose, size, and chemical composition," *Nanotoxicology*, vol. 9, no. 5, pp. 591–602, 2015.

[18] K. Unfried, C. Albrecht, L.-O. Klotz, A. von Mikecz, S. Grether-Beck, and R. P. F. Schins, "Cellular responses to nanoparticles: target structures and mechanisms," *Nanotoxicology*, vol. 1, no. 1, pp. 52–71, 2009.

[19] T. L. Hwang, C. Y. Hsu, I. A. Aljuffali, C. H. Chen, Y. T. Chang, and J. Y. Fang, "Cationic liposomes evoke proinflammatory mediator release and neutrophil extracellular traps (NETs) toward human neutrophils," *Colloids and Surfaces B: Biointerfaces*, vol. 128, pp. 119–126, 2015.

[20] P. R. Lockman, J. M. Koziara, R. J. Mumper, and D. D. Allen, "Nanoparticle surface charges alter blood–brain barrier integrity and permeability," *Journal of Drug Targeting*, vol. 12, no. 9-10, pp. 635–641, 2004.

[21] D. F. Moyano, Y. Liu, F. Ayaz et al., "Immunomodulatory effects of coated gold nanoparticles in LPS-stimulated in vitro and in vivo murine model systems," *Chem*, vol. 1, no. 2, pp. 320–327, 2016.

[22] M. Bartneck, H. A. Keul, G. Zwadlo-Klarwasser, and J.. Groll, "Phagocytosis independent extracellular nanoparticle clearance by human immune cells," *Nano Letters*, vol. 10, no. 1, pp. 59–63, 2010.

[23] D. B. Warheit, B. R. Laurence, K. L. Reed, D. H. Roach, G. A. Reynolds, and T. R. Webb, "Comparative pulmonary toxicity assessment of single-wall carbon nanotubes in rats," *Toxicological Sciences*, vol. 77, no. 1, pp. 117–125, 2004.

[24] S. Tomić, J. Đokić, S. Vasilijić et al., "Size-dependent effects of gold nanoparticles uptake on maturation and antitumor functions of human dendritic cells in vitro," *PLoS One*, vol. 9, no. 5, article e96584, 2014.

[25] C. P. García, V. Sumbayev, D. Gilliland et al., "Microscopic analysis of the interaction of gold nanoparticles with cells of the innate immune system," *Scientific Reports*, vol. 3, no. 1, article 1326, 2013.

[26] A. K. Patri, A. Myc, J. Beals, T. P. Thomas, N. H. Bander, and J. R. Baker, "Synthesis and in vitro testing of J591 antibody –dendrimer conjugates for targeted prostate cancer therapy," *Bioconjugate Chemistry*, vol. 15, no. 6, pp. 1174–1181, 2004.

[27] V. Guillemard and H. U. Saragovi, "Taxane-antibody conjugates afford potent cytotoxicity, enhanced solubility, and tumor target selectivity," *Cancer Research*, vol. 61, no. 2, pp. 694–699, 2001.

[28] R. Shukla, N. Chanda, A. Zambre et al., "Laminin receptor specific therapeutic gold nanoparticles (^{198}AuNP-EGCg) show efficacy in treating prostate cancer," *Proceedings of the National Academy of Sciences of the United States of America*, vol. 109, no. 31, pp. 12426–12431, 2012.

[29] S. S. Chang, P. B. Gaudin, V. E. Reuter, and W. D. W. Heston, "Prostate-specific membrane antigen: present and future applications," *Urology*, vol. 55, no. 5, pp. 622–629, 2000.

[30] R. S. Israeli, C. T. Powell, J. G. Corr, W. R. Fair, and W. D. Heston, "Expression of the prostate-specific membrane antigen," *Cancer Research*, vol. 54, no. 7, pp. 1807–1811, 1994.

[31] A. Y. Al-Yasiri, M. Khoobchandani, C. S. Cutler et al., "Mangiferin functionalized radioactive gold nanoparticles (MGF-^{198}AuNPs) in prostate tumor therapy: green nanotechnology for production, in vivo tumor retention and evaluation of therapeutic efficacy," *Dalton Transactions*, vol. 46, no. 42, pp. 14561–14571, 2017.

[32] R. Rattan, S. Bhattacharjee, H. Zong et al., "Nanoparticle-macrophage interactions: a balance between clearance and cell-specific targeting," *Bioorganic & Medicinal Chemistry*, vol. 25, no. 16, pp. 4487–4496, 2017.

[33] N. Lewinski, V. Colvin, and R. Drezek, "Cytotoxicity of nanoparticles," *Small*, vol. 4, no. 1, pp. 26–49, 2008.

[34] I. M. M. Paino and V. Zucolotto, "Poly(vinyl alcohol)-coated silver nanoparticles: activation of neutrophils and nanotoxicology effects in human hepatocarcinoma and mononuclear cells," *Environmental Toxicology and Pharmacology*, vol. 39, no. 2, pp. 614–621, 2015.

[35] K. Babin, D. M. Goncalves, and D. Girard, "Nanoparticles enhance the ability of human neutrophils to exert phagocytosis by a Syk-dependent mechanism," *Biochimica et Biophysica Acta*, vol. 1850, no. 11, pp. 2276–2282, 2015.

[36] L. Lu, K. Li, Y. H. Mao et al., "Gold-chrysophanol nanoparticles suppress human prostate cancer progression through inactivating AKT expression and inducing apoptosis and ROS generation in vitro and in vivo," *International Journal of Oncology*, vol. 51, no. 4, pp. 1089–1103, 2017.

[37] G. Oberdörster, E. Oberdörster, and J. Oberdörster, "Nanotoxicology: an emerging discipline evolving from studies of ultrafine particles," *Environmental Health Perspectives*, vol. 113, no. 7, pp. 823–839, 2005.

[38] J. C. Evans, M. Malhotra, J. Guo et al., "Folate-targeted amphiphilic cyclodextrin. siRNA nanoparticles for prostate cancer therapy exhibit PSMA mediated uptake, therapeutic gene silencing in vitro and prolonged circulation in vivo," *Nanomedicine*, vol. 12, no. 8, pp. 2341–2351, 2016.

[39] R. Thangapazham, A. Puri, S. Tele, R. Blumenthal, and R. Maheshwari, "Evaluation of a nanotechnology-based carrier for delivery of curcumin in prostate cancer cells," *International Journal of Oncology*, vol. 32, no. 5, pp. 1119–1123, 2008.

[40] E. Oh, J. B. Delehanty, K. E. Sapsford et al., "Cellular uptake and fate of PEGylated gold nanoparticles is dependent on both cell-penetration peptides and particle size," *ACS Nano*, vol. 5, no. 8, pp. 6434–6448, 2011.

[41] K. Rahme, M. T. Nolan, T. Doody et al., "Highly stable PEGylated gold nanoparticles in water: applications in biology and catalysis," *RSC Advances*, vol. 3, no. 43, p. 21016, 2013.

[42] S. L. Chen, S. C. Wang, C. J. Ho et al., "Prostate cancer mortality-to-incidence ratios are associated with cancer care disparities in 35 countries," *Scientific Reports*, vol. 7, no. 1, p. 40003, 2017.

[43] M. C. Woodle, M. S. Newman, and J. A. Cohen, "Sterically stabilized liposomes: physical and biological properties," *Journal of Drug Targeting*, vol. 2, no. 5, pp. 397–403, 1994.

[44] C. Peetla and V. Labhasetwar, "Effect of molecular structure of cationic surfactants on biophysical interactions of surfactant-modified nanoparticles with a model membrane and cellular uptake," *Langmuir*, vol. 25, no. 4, pp. 2369–2377, 2009.

[45] C. R. Miller, B. Bondurant, S. D. McLean, K. A. McGovern, and D. F. O'Brien, "Liposome-cell interactions in vitro: effect of liposome surface charge on the binding and endocytosis of conventional and sterically stabilized liposomes," *Biochemistry*, vol. 37, no. 37, pp. 12875–12883, 1998.

[46] T. L. Hwang, C. T. Sung, I. A. Aljuffali, Y. T. Chang, and J. Y. Fang, "Cationic surfactants in the form of nanoparticles and micelles elicit different human neutrophil responses: a toxicological study," *Colloids and Surfaces. B, Biointerfaces*, vol. 114, pp. 334–341, 2014.

[47] H. Collet, E. Souaid, H. Cottet et al., "An expeditious multigram-scale synthesis of lysine dendrigraft (DGL) polymers by aqueous *N*-carboxyanhydride polycondensation," *Chemistry - A European Journal*, vol. 16, no. 7, pp. 2309–2316, 2010.

[48] M. B. Gorbet and M. V. Sefton, "Endotoxin: the uninvited guest," *Biomaterials*, vol. 26, no. 34, pp. 6811–6817, 2005.

[49] Y. Li, M. Fujita, and D. Boraschi, "Endotoxin contamination in nanomaterials leads to the misinterpretation of immunosafety results," *Frontiers in Immunology*, vol. 8, p. 472, 2017.

[50] B. W. Neun and M. A. Dobrovolskaia, "Considerations and some practical solutions to overcome nanoparticle interference with LAL assays and to avoid endotoxin contamination in nanoformulations," *Methods in Molecular Biology*, vol. 1682, pp. 23–33, 2018.

[51] Ã. França, B. Pelaz, M. Moros et al., "Sterilization matters: consequences of different sterilization techniques on gold nanoparticles," *Small*, vol. 6, no. 1, pp. 89–95, 2010.

[52] D. A. Giljohann, D. S. Seferos, W. L. Daniel, M. D. Massich, P. C. Patel, and C. A. Mirkin, "Gold nanoparticles for biology

and medicine," *Angewandte Chemie International Edition*, vol. 49, no. 19, pp. 3280–3294, 2010.

[53] K. Rahme, L. Chen, R. G. Hobbs, M. A. Morris, C. O'Driscoll, and J. D. Holmes, "PEGylated gold nanoparticles: polymer quantification as a function of PEG lengths and nanoparticle dimensions," *RSC Advances*, vol. 3, no. 17, pp. 6085–6094, 2013.

[54] P. Gómez-Ochoa, A. Lara, G. Couto et al., "The nitroblue tetrazolium reduction test in canine leishmaniosis," *Veterinary Parasitology*, vol. 172, no. 1-2, pp. 135–138, 2010.

[55] P. Gómez-Ochoa, D. Sabate, J. Homedes, and L. Ferrer, "Use of the nitroblue tetrazolium reduction test for the evaluation of Domperidone effects on the neutrophilic function of healthy dogs," *Veterinary Immunology and Immunopathology*, vol. 146, no. 1, pp. 97–99, 2012.

[56] D. G. Nathan, R. L. Baehner, and D. K. Weaver, "Failure of nitro blue tetrazolium reduction in the phagocytic vacuoles of leukocytes in chronic granulomatous disease," *Journal of Clinical Investigation*, vol. 48, no. 10, pp. 1895–1904, 1969.

[57] V. Kononenko, M. Narat, and D. Drobne, "Nanoparticle interaction with the immune system," *Arhiv za Higijenu Rada i Toksikologiju*, vol. 66, no. 2, pp. 97–108, 2015.

[58] P. Kruger, M. Saffarzadeh, A. N. R. Weber et al., "Neutrophils: between host defence, immune modulation, and tissue injury," *PLoS Pathogens*, vol. 11, no. 3, article e1004651, 2015.

[59] L. Fialkow, Y. Wang, and G. P. Downey, "Reactive oxygen and nitrogen species as signaling molecules regulating neutrophil function," *Free Radical Biology & Medicine*, vol. 42, no. 2, pp. 153–164, 2007.

[60] V. Brinkmann, U. Reichard, C. Goosmann et al., "Neutrophil extracellular traps kill bacteria," *Science*, vol. 303, no. 5663, pp. 1532–1535, 2004.

[61] I. Durocher, C. Noël, V. Lavastre, and D. Girard, "Evaluation of the in vitro and in vivo proinflammatory activities of gold (+) and gold (−) nanoparticles," *Inflammation Research*, vol. 66, no. 11, pp. 981–992, 2017.

[62] A. W. Segal and A. J. Levi, "Cell damage and dye reduction in the quantitative nitroblue tetrazolium (NBT) test," *Clinical and Experimental Immunology*, vol. 19, no. 2, pp. 309–318, 1975.

[63] A. Fattorossi, R. Nisini, S. le Moli, G. de Petrillo, and R. D'Amelio, "Flow cytometric evaluation of nitro blue tetrazolium (NBT) reduction in human polymorphonuclear leukocytes," *Cytometry*, vol. 11, no. 8, pp. 907–912, 1990.

[64] J. Guo, C. M. O'Driscoll, J. D. Holmes, and K. Rahme, "Bioconjugated gold nanoparticles enhance cellular uptake: a proof of concept study for siRNA delivery in prostate cancer cells," *International Journal of Pharmaceutics*, vol. 509, no. 1-2, pp. 16–27, 2016.

[65] M. Iwasaka, J. Miyakoshi, and S. Ueno, "Optical absorbance of hemoglobin and red blood cell suspensions under magnetic fields," *IEEE Transactions on Magnetics*, vol. 37, no. 4, pp. 2906–2908, 2001.

[66] Z. J. Deng, M. Liang, I. Toth, M. Monteiro, and R. F. Minchin, "Plasma protein binding of positively and negatively charged polymer-coated gold nanoparticles elicits different biological responses," *Nanotoxicology*, vol. 7, no. 3, pp. 314–322, 2013.

[67] D. Hühn, K. Kantner, C. Geidel et al., "Polymer-coated nanoparticles interacting with proteins and cells: focusing on the sign of the net charge," *ACS Nano*, vol. 7, no. 4, pp. 3253–3263, 2013.

[68] B. D. Chithrani, A. A. Ghazani, and W. C. W. Chan, "Determining the size and shape dependence of gold nanoparticle uptake into mammalian cells," *Nano Letters*, vol. 6, no. 4, pp. 662–668, 2006.

[69] S. H. De Paoli Lacerda, J. J. Park, C. Meuse et al., "Interaction of gold nanoparticles with common human blood proteins," *ACS Nano*, vol. 4, no. 1, pp. 365–379, 2010.

[70] N. M. Goldenberg and B. E. Steinberg, "Surface charge: a key determinant of protein localization and function," *Cancer Research*, vol. 70, no. 4, pp. 1277–1280, 2010.

[71] P. Perret, S. Bacot, A. Gèze et al., "Biodistribution and preliminary toxicity studies of nanoparticles made of biotransesterified β–cyclodextrins and PEGylated phospholipids," *Materials Science and Engineering: C*, vol. 85, pp. 7–17, 2018.

[72] K. R. Chaudhari, M. Ukawala, A. S. Manjappa et al., "Opsonization, biodistribution, cellular uptake and apoptosis study of PEGylated PBCA nanoparticle as potential drug delivery carrier," *Pharmaceutical Research*, vol. 29, no. 1, pp. 53–68, 2012.

[73] D. E. Owens III and N. A. Peppas, "Opsonization, biodistribution, and pharmacokinetics of polymeric nanoparticles," *International Journal of Pharmaceutics*, vol. 307, no. 1, pp. 93–102, 2006.

[74] R. D. Vinluan III and J. Zheng, "Serum protein adsorption and excretion pathways of metal nanoparticles," *Nanomedicine*, vol. 10, no. 17, pp. 2781–2794, 2015.